Dual-Loop Model of the Human Controller

R. A. Hess*
NASA Ames Research Center, Moffett Field, Calif.

A dual-loop model of the human controller in single-axis compensatory tracking tasks is introduced. This model possesses an inner-loop closure that involves feeding back that portion of controlled element output rate that is due to control activity. A novel feature of the model is the explicit appearance of the human's internal representation of the manipulator-controlled element dynamics in the inner loop. The sensory inputs to the human controller are assumed to be system error and control force. The former can be sensed via visual, aural, or tactile displays, whereas the latter is assumed to be sensed in kinesthetic fashion. A set of general adaptive characteristics for the model is hypothesized, including a method for selecting simplified internal models of the manipulator-controlled element dynamics. It is demonstrated that the model can produce controller describing functions that closely approximate those measured in four laboratory tracking tasks in which the controlled element dynamics vary considerably in terms of ease of control. An empirically derived expression for the normalized injected error remnant spectrum is introduced.

Introduction

Single-Loop Model

FIGURE 1 is a simplified block diagram representation of a single-axis compensatory tracking task in which a human controller is attempting to maintain a controlled element at some specified equilibrium point. The controller views a display of system error (difference between actual and desired controlled element output) and uses a manipulator to generate input signals to the controlled element to drive the error to zero. Figure 2 shows the classical quasilinear representation of human controller dynamics in the task of Fig. 1. Such quasilinear models consisting of a describing function Y_p and a remnant signal n_e have provided the analytical basis for the vast majority of studies of systems under continuous manual control. Measurements of Y_p and the power spectral density of n_e have been undertaken and reported for tasks involving a wide variety of controlled elements, disturbance characteristics, and manipulators.[1,2]

To the author's knowledge, all the measurements of human controller dynamics in single-axis tasks have been predicated on the "single-loop" model of Fig. 2. This model has been employed because of its structural simplicity. The classical spectral techniques used in identifying controller dynamics are not capable of verifying more complex model structures under the restrictions implicit in Fig. 1, i.e., one disturbance and one manipulator.[3]

Dual-Loop Model

It is the thesis of the research to be described that a more representative model of the actual signal-processing structure of the human controller should exhibit an internal feedback loop that is not evident in the single-loop models now in common use. As will be seen, this hypothetical inner-loop involves a neuromuscular command signal derived from the rate of change of controlled element output which is due to human control activity. It is not the author's contention that the single-loop human controller models now in use are in any way incorrect, but rather that they contain an implicit but important internal loop closure which, if explicitly considered, can account for a good deal of the adaptive nature of the human controller in a systematic manner.

Figure 3 is a block diagram representation of the hypothetical human controller model just alluded to. This model will be referred to as the "dual-loop" model of the human controller to distinguish it from the single-loop structure of Fig. 2. The dual-loop model was not derived from any physiological imperatives, but rather stems from a structurally similar but philosophically different model developed by Smith and discussed in Ref. 4 and later in Ref. 5. In his work, Smith pointed out that a model similar to that shown in Fig. 3 could explain the manner in which a human controller adapts to different controlled element dynamics. The primary difference between the model discussed here and that developed by Smith is that the latter model assumes that controlled element output rate due to control activity is a quantity *sensed directly* through a *visual* sensory input. For this rate to be sensed directly, however, certain restrictive assumptions must be made regarding the bandwidth of the time rate of change of the input or disturbance. In the model that is the subject of this paper, it is assumed that controlled

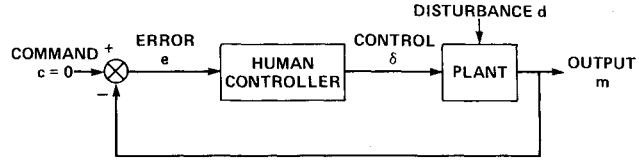

Fig. 1 Single-axis compensatory tracking task.

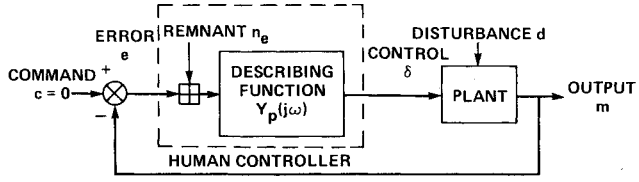

Fig. 2 Quasilinear model of the human controller.

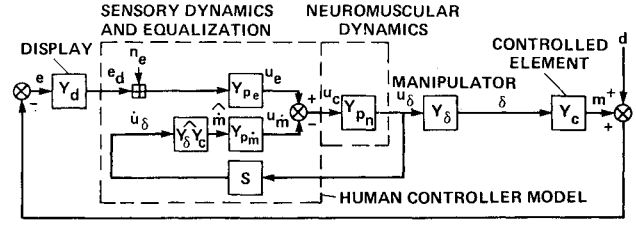

Fig. 3 Quasilinear dual-loop model of the human controller.

Received Aug. 29, 1977; revision received Jan. 23, 1978.
Index category: Handling Qualities, Stability and Control.
*Research Scientist. Member AIAA.

element output rate due to control activity is a quantity *derived* from a *kinesthetic* sensory input. Although this assumption demands a literal interpretation of the inner-loop equalization of Fig. 3 that is not required in Smith's model, no restriction need be placed upon the bandwidth of the input rate or disturbance rate. Indeed, it will be shown that the need for assuming any error rate perception in the model at all will be minimized or completely eliminated. Thus, the model discussed here is directly applicable to the study of tracking tasks involving aural or tactile displays where the assumption of direct error rate perception is considerably more tenuous than in the case of visual displays.

Dual-Loop Model Specifics

Parametrization

The sensory inputs to the human in the model of Fig. 3 are displayed error e_d and control force u_δ. The sensory modality for displayed error can be visual, aural, or tactile. Since u_δ is considered a control *force* applied by the human to the manipulator, u_δ is assumed to be sensed primarily by the Golgi tendon organs and the muscle spindles in the particular limb driving the manipulator.[6]

The disturbance signal in Fig. 3 is shown injected into controlled element output for the sake of generality. In this way, the structure can represent a command input tracking task {(d = (-command input)} or a disturbance regulation task (d = disturbance). Although changes in input/disturbance spectral characteristics can be important, they have considerably less influence on human controller dynamics than the changes in controlled element dynamics that will be encountered in this research. Hence, such input/disturbance effects will not be treated here.

The function of the inner loop in the model of Fig. 3 is to feedback equalized output rate $u_{\dot m}$ to the neuromuscular system. It is this feedback loop that immediately distinguishes the model from the single-loop structure of Fig. 2. The remaining neuromuscular signal is equalized error u_e. The injected remnant signal n_e is included to account for nonlinearities and/or time variations in quasilinear fashion. The parameters associated with the model of Fig. 3 are presented in Table 1.

The equalization Y_{p_e} contains a gain, a simple first-order lead term, and a pure time delay τ. The element $Y_{\hat\delta} Y_c$ represents the human controller's internal model of the manipulator-controlled element dynamics. The equalization $Y_{p_{\dot m}}$ consists of a gain and a low-frequency washout, where

Table 1 Dual-loop model parameters

Expression	Description
$Y_{p_e} = K_e (T_L s + 1) e^{-\tau s}$	Displayed error equalization
$Y_{p_{\dot m}} = \dfrac{K_{\dot m} [(T_{\dot m}/\lvert T_{\dot m}\rvert) s]^k}{(T_{\dot m} s + 1)^k}$	Control-rate equalization, $k = 1, 2, \ldots$
$Y_{\hat\delta} Y_c$	Human controller's internal model of manipulator-controlled element dynamics
$Y_{p_n} = \dfrac{1}{\left(\dfrac{s}{\omega_n}\right)^2 + \dfrac{2\zeta_n}{\omega_n} s + 1}$	Neuromuscular dynamics
n_e	Remnant injected into displayed error
$Y_p = \dfrac{u_\delta}{e_d} = \dfrac{Y_{p_e} Y_{p_n}}{1 + Y_{p_n} Y_{\hat\delta} Y_c Y_{p_{\dot m}} s}$	Equivalent single-loop human controller-describing function

"low frequency" refers to frequencies well below the open-loop crossover frequency ω_c. The ratio $T_{\dot m}/\lvert T_{\dot m}\rvert = 1$s in $Y_{p_{\dot m}}$ merely serves to nondimsionalize the washout dynamics. The integer exponent k is included to implement sharper washout characteristics, if necessary. The element Y_{p_n} represents the neuromuscular dynamics of the particular limb which drives the manipulator. With the inner loop of Fig. 3 closed, the simple quadratic form for Y_{p_n} shown in Table 1 can exhibit the salient features of measured high-frequency human controller dynamics, namely, a typically subcritical damping ratio $\zeta_{n_{CL}}$, and a minimum second-order amplitude fall-off beyond the undamped natural frequency $\omega_{n_{CL}}$. As mentioned previously, the injected remnant signal n_e is part of the quasilinear representation of the human controller.

Adaptive Characteristics

Implicit in the dual-loop formulation is the assumption that the structure as outlined in Table 1 is complete; i.e., no additions must be made or restructuring undertaken to account for human controller adaptation to various controlled elements, displays, manipulators, etc. The adaptive potential of the model is contained in the parameters of the inner- and outer-loop equalization and in the internal manipulator-controlled element model $Y_{\hat\delta} Y_c$. Indeed, the dominant adaptive feature of the dual-loop model is the explicit appearance of $Y_{\hat\delta} Y_c$ in the equivalent single-loop form of the model in Table 1 (Y_p). Five hypotheses regarding the general adaptive characteristics of the parametrized dual-loop human controller model are now offered:

Hypothesis 1

The parameters K_e, $K_{\dot m}$, and $T_{\dot m}$ act in consort with the internal model of the manipulator-controlled element dynamics $Y_{\hat\delta} Y_c$ to define the essential adaptive capabilities of the dual-loop model. The parameter T_L in Y_{p_e} is used only when K_e, $K_{\dot m}$, $T_{\dot m}$, and $Y_{\hat\delta} Y_c$ themselves are unable to provide the effective lead equalization that may be required in a specific task.

Hypothesis 2

The relative utilization of the inner and outer loops of the dual-loop model is a function of manipulator-controlled element dynamics and the quality of the sensory inputs e_d and u_δ.

Hypothesis 3

Relative loop utilization in the dual-loop model can be quantified by the ratio $K_{\dot m}/K_e$.

Hypothesis 4

The value of $T_{\dot m}$ is determined by the extent to which the inner loop is utilized. The more the inner loop is utilized, the larger the value of $T_{\dot m}$.

Hypothesis 5

The transfer function $\hat m/u_\delta$, which describes part of the equalization activity in the inner loop of the dual-loop model, is of the form: $\hat m/u_\delta = sY_{\hat\delta} Y_c = sK_s s^n$, $n = 0, \pm 1, \pm 2, \ldots$, etc. The frequency characteristics of $Y_{\hat\delta} Y_c$ in the region beyond the open-loop crossover frequency, yield values for K_s and n.

No hypotheses regarding the adaptive nature of the parameters τ, ζ_n, and ω_n are offered. These parameters affect primarily the high-frequency portion of the controller describing function Y_p ($\omega > 10$ rad/s). Since measured data tend to be scant in this frequency range, verifying hypotheses regarding parameter variations would be difficult.

As mentioned previously, the inner-loop equalization of the dual-loop model must be interpreted in a more literal sense

than that of Smith's model, which assumes visual stimuli alone. In terms of adaptive behavior, the most important inner-loop element is probably $Y_{\dot{\delta}}Y_c$, the internal model of the manipulator-controlled element dynamics. It is difficult to make a strong argument for the existence of the internal model on strictly physiological grounds; however, it is worth noting that other human controller models have utilized internal representations of the controlled element with success.[7] The internal model simplification inherent in hypothesis 5 can certainly make the internal model concept more palatable, since it implies that from the dual-loop model standpoint, the human generates $\hat{m}(t)$ by integrating, differentiating, or multiplying by a constant, the sensed control force $u_\delta(t)$. In this context, the simplified internal model $Y_{\dot{\delta}}Y_c$ merely serves to determine which of these time domain operations are appropriate for the manipulator-controlled element dynamics at hand.

Describing Function Expressions

The last equation in Table 1 is an expression for the equivalent single-loop human controller describing function Y_p in terms of the dual-loop entities Y_{pe}, $Y_{p\dot{m}}$, Y_{pn}, and $Y_{\dot{\delta}}Y_c$. By utilizing this equation and the remaining relations in Table 1, the following describing function expressions can be obtained.

Small-Bandwidth Approximation

With $k=1$ and with the simplifying approximations $\tau=0$, $Y_{pn}=1.0$, then

$$Y_p=\frac{u_\delta}{e_d}=\frac{K_e(T_{\dot{m}}s+1)\ (T_Ls+1)}{(K_{\dot{m}}Y_{\dot{\delta}}Y_cT_{\dot{m}}/|T_{\dot{m}}|)s^2+(T_{\dot{m}})s+1} \quad (1)$$

Large-Bandwidth Approximation

With $k=1$ and without the previous simplifying approximations, then

$$Y_p=u_\delta/e_d=K_e(T_{\dot{m}}s+1)\ (T_Ls+1)e^{-\tau s}/\frac{T_{\dot{m}}}{\omega_n^2}s^3$$

$$+\left(\frac{2\zeta_nT_{\dot{m}}}{\omega_n}+\frac{K_{\dot{m}}Y_{\dot{\delta}}Y_cT_{\dot{m}}}{|T_{\dot{m}}|}+\frac{1}{\omega_n^2}\right)s^2+\left(T_{\dot{m}}+\frac{2\zeta_n}{\omega_n}\right)s+1 \quad (2)$$

As will be seen, Eqs. (1) and (2) and the general guidelines of the five hypotheses just stated allow rapid "identification" of dual-loop model parameters using measured describing function data through the following two-step process. First, K_e, $K_{\dot{m}}$, $T_{\dot{m}}$, and, if necessary, T_L are selected using Eq. (1) and the low- to mid-frequency ($\omega\leq\omega_c$) describing function data. Second, ζ_n, ω_n, and τ are chosen using Eq. (2), the selected values of K_e, $K_{\dot{m}}$, $T_{\dot{m}}$, and T_L, and the high-frequency ($\omega>\omega_c$) describing function data. Obviously, this procedure does not constitute rigorous identification of the dual-loop model in the sense of obtaining a minimum set of unique model parameter estimates with each controlled element under consideration. However, the procedure does allow one to demonstrate that the dual-loop model parameters can be selected in a straightforward manner to match experimentally derived human controller-describing functions across a wide spectrum of controlled element dynamics. In addition, the variation of these parameters across the spectrum of controlled elements will be shown to be orderly and consistent with the five hypotheses stated above.

Model Validation

The dual-loop model can produce describing functions that closely approximate those measured in experimental tracking tasks while fulfilling the explicit and implicit constraints of the five hypotheses outlined previously. The four tracking tasks to be considered employ controlled element dynamics of K, K/s, K/s^2, and $K/s\ (s-1)$. As documented in Ref. 8, these elements represent increasingly difficult dynamics for the human to control. The measured describing functions for the K, K/s, and K/s^2 dynamics were taken from Ref. 7. The $K/s\ (s-1)$ data were taken from Ref. 9. All of the manipulators used in the four experimental tasks were isometric (force) devices. Thus, manipulator dynamics can be considered negligible as can display dynamics.

The model parameter "identification" was carried out using the small- and large-bandwidth approximations discussed previously. In each case, the model was hand-fitted to the data. The first four rows of Table 2 summarize the results. Figures 4 through 7 compare the experimentally derived describing functions with those obtained with the dual-loop model when the parameters of Table 2 were used. Figures 8 and 9 show the orderly variation of $K_{\dot{m}}/K_e$ and $1/T_{\dot{m}}$ as the controlled elements become increasingly difficult to control as documented in Ref. 8.

Discussion

As Figs. 4-7 show, the measured and model-generated describing functions compare quite well. The $K/s(s-1)$ dynamics required sharper washout characteristic in the dual-loop model than did the other dynamics, i.e., the k value of Table 1 was set to 3. Also, in this case, a simplified internal model of the manipulator-controlled element dynamics was employed, namely, $Y_{\dot{\delta}}Y_c=2.82/s^2$. This provided an accurate representation of the actual unstable dynamics for frequencies beyond open-loop crossover. In addition, a modicum of actual error rate utilization ($T_L=0.3$ s) was required for the unstable dynamics. This was not true for the K/s^2 dynamics, where the apparent "error lead equalization" in the dual-loop describing function results are obtained from inner-loop activity alone. Likewise, the apparent "error lag equalization" for the K dynamics is accomplished by inner-loop activity. This ability of the model structure of Fig. 3 to produce apparent lead and lag equalization by inner-loop activity was first pointed out by Smith.[4,5]

It is interesting to note that the documented increments in high-frequency phase lag (or effective time delay τ_e) associated with tasks requiring increased amounts of error lead equalization can be explained via the dual-loop model. Figures 10 and 11 show the root locus diagrams for the inner-loop closure of the dual-loop model for K/s and K/s^2 controlled element dynamics. The closed-loop root locations correspond to the model parameters shown in Table 2. A close examination of the diagrams reveals that $K_{\dot{m}}$ and $T_{\dot{m}}$ play a

Table 2 Summary of dual-loop modeling results

$Y_\delta Y_c$	$Y_{\dot{\delta}}Y_c$	K_e	T_L,s	$K_{\dot{m}}$,s	$T_{\dot{m}}$,s	τ,s	ζ_n	ω_n,rad/s
1.0	1.0	2.5	0	0.5	1.0	0.1	0.1	20
$1/s$	$1/s$	18.0	0	6.0	2.0	0.13	0.3	15
$1/s^2$	$1/s^2$	26.5	0	32.3	3.33	0.16	0.7	15
$2.82/s(s-1)$[a]	$2.82/s^2$	5.5	0.33	10.0	5.0	0.15	0.1	15
$145/\Delta$[b]	$10/s^2$	1.4	0	1.0	1.25	0.19	0.7	15
$2/s-2$	$2/s$	18.0	0	7.0	3.33	0.11	–	–

[a] Higher order controller model used ($k=3$ in Table 1). [b] $\Delta=s^3+12.3s^2+11.6s$.

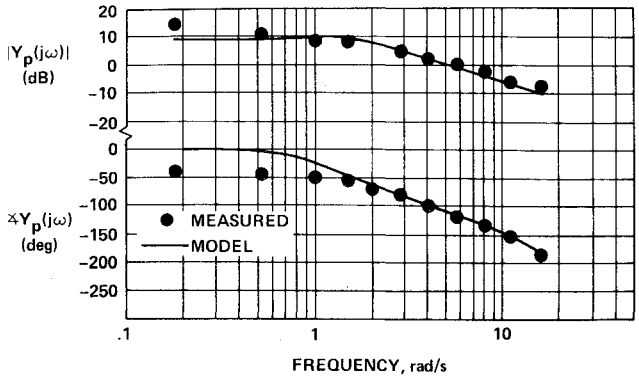

Fig. 4 Measured and dual-loop model describing functions for K dynamics.

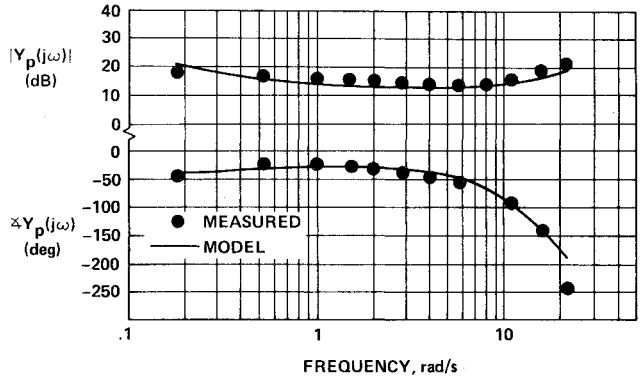

Fig. 5 Measured and dual-loop model describing functions for K/s dynamics.

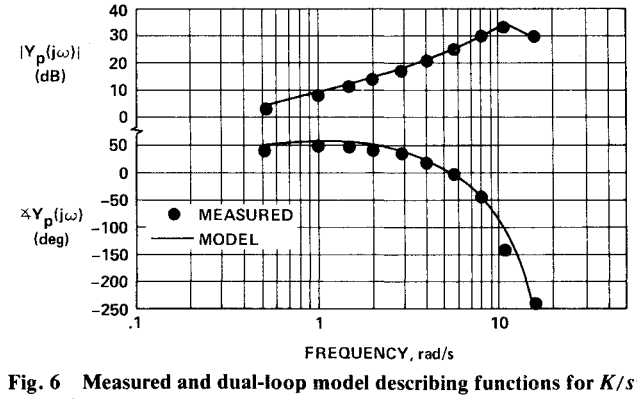

Fig. 6 Measured and dual-loop model describing functions for K/s^2 dynamics.

dominant role in determining the positions of the closed-loop roots of the neuromuscular mode (those closed-loop roots emanating from the open-loop quadratic neuromuscular pair). The position of these closed-loop roots, in turn, influences the magnitude of the high-frequency phase lag in the describing function. In particular, the relatively low value of $\omega_{n_{CL}}$ in Fig. 11 causes an increased phase lag to appear in the human controller model over and above the slight increase attributable to the increment in τ noted in Table 2. Note also that the larger lag for the K/s^2 controlled element is not attributable to the position of the *open-loop* neuromuscular quadratic pair relative to that for the K/s element. Thus, in terms of a "crossover" human controller model that subsumes high-frequency describing function characteristics into an effective time delay τ_e,[1] the K/s^2 dynamics will appear to induce a larger τ_e than the K/s dynamics.

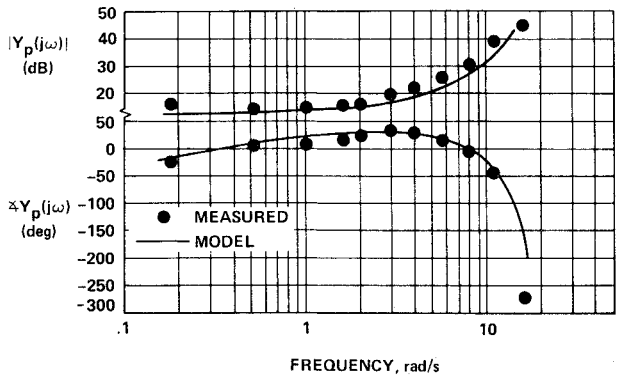

Fig. 7 Measured and dual-loop model describing functions for d) $K/s\,(s-1)$ dynamics

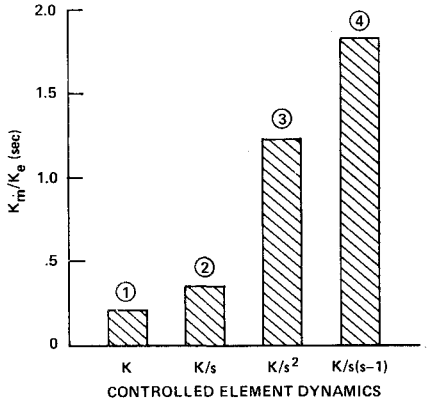

ⓝ "DEGREE OF EFFORT" EXPENDED IN CONTROLLING K, K/s, K/s² AND K/s(s-1) DYNAMICS AS DOCUMENTED IN REFERENCE 8,
① = LEAST EFFORT

Fig. 8 K_m/K_e for various controlled element dynamics.

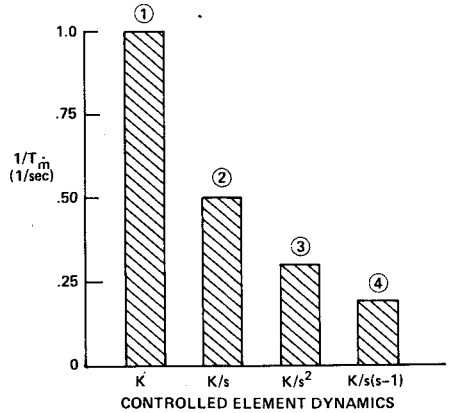

ⓝ "DEGREE OF EFFORT" EXPENDED IN CONTROLLING K, K/s, K/s² AND K/s(s-1) DYNAMICS AS DOCUMENTED IN REFERENCE 8,
① = LEAST EFFORT

Fig. 9 $1/T_m$ for various controlled element dynamics.

Finally, note that the dual-loop model correctly generates the low-frequency phase lag apparent in the measured data for K/s dynamics. This success is somewhat offset by the poor low-frequency phase comparison for the K dynamics, but is nonetheless, worthy of note.

Remnant Model

An empirical expression for the normalized power spectral density of the remnant that is injected into the displayed error

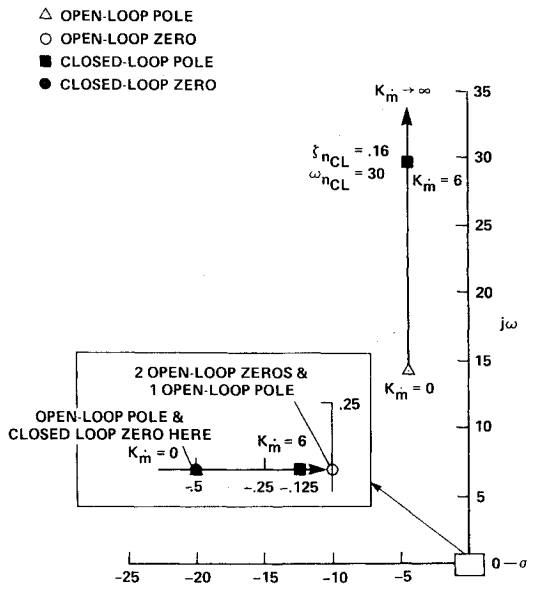

Fig. 10 Loci of closed-loop poles of δ/u_e as a function of $K_{\dot m}$; K/s^2 dynamics.

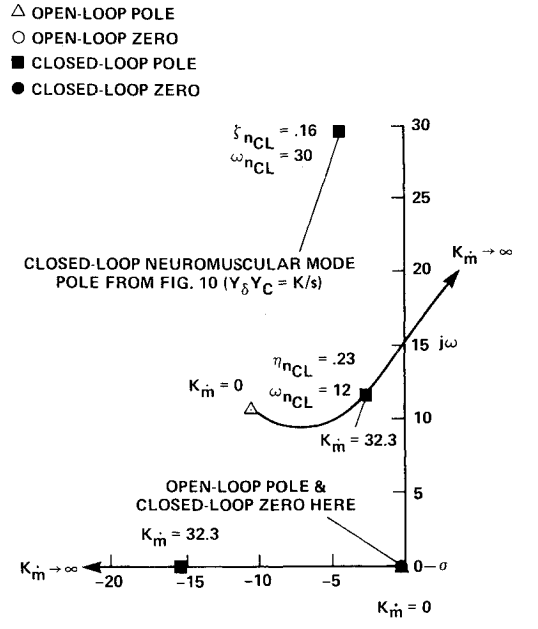

Fig. 11 Loci of closed-loop poles of δ/u_e as a function of $K_{\dot m}$; K/s^2 dynamics.

of the dual-loop model was obtained from the measured remnant data as

$$\frac{\Phi_{nn_e}}{\sigma_e^2} = \frac{P_e(K_{\dot m}/K_e)}{1 + (K_{\dot m}/K_e)^2\omega^2/2}$$

where σ_e is the root-mean-square value of the displayed error signal and P_e is a parameter to account for the fact that different levels of human controller attention are required for different control tasks. Only two values of P_e were needed to match the measured remnant data: $P_e = 0.2$ to represent a "low" attention level and $P_e = 0.04$ to represent a "high" attention level. Based upon what is known about human ability to allocate attention to a given task, it is highly probable that a continuum of attention levels would be implied by a data base larger than that used here.

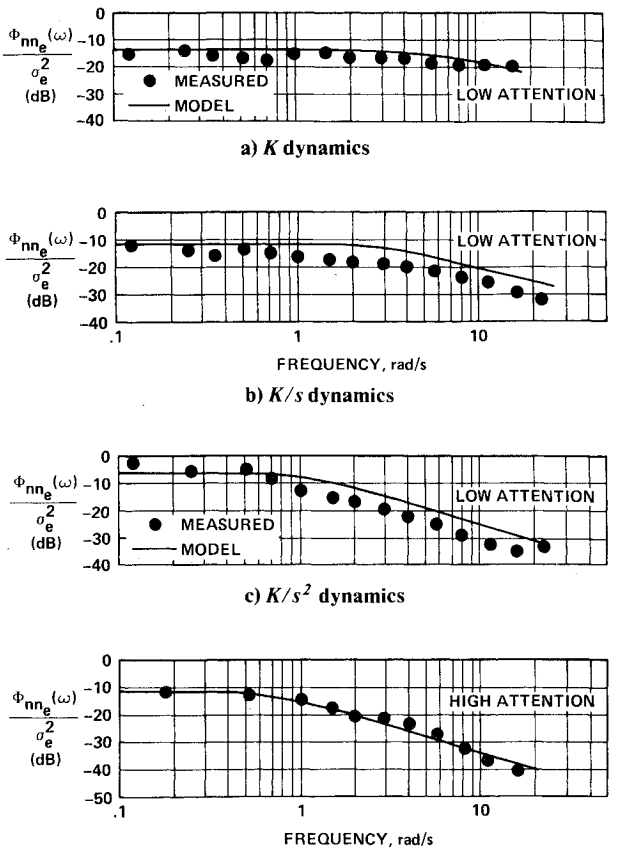

Fig. 12 Measured and empirical injected remnant spectra.

Although the experimental remnant spectra for the K/s^2 and $K/s(s-1)$ dynamics were based upon remnant injected into error *rate*, the author related these spectra to equivalent remnant injected into error. Figures 12a-d compare the measured and empirical remnant spectra for the four controlled element dynamics under study. As can be seen, the comparison is quite favorable. Note that for the remnant power spectra, the decibel is defined as 10 log (•).

Internal Model Simplification

The two preceding sections demonstrate that the proposed dual-loop model can produce human controller-describing functions closely approximating those measured in a series of four tracking tasks. These tasks varied considerably in terms of ease of control. The ability of an empirical remnant model to match the experimentally derived injected remnant spectra was also indicated. It is of interest, however, to explore the issue of internal model simplification (hypothesis 5) a bit further. To this end, the frequency domain data from a pair of tracking tasks reported in Refs. 10 and 11 were utilized. The controlled element dynamics in these tasks were of the form $K/(s^3 + 12.3s^2 + 11.6s)$ and $K/s-2$, respectively. As stated in hypothesis 5, these dynamics should be simplified by fitting approximations of the form $Y_{\hat\delta} Y_c = K_s s^n$ to the actual frequency characteristics of $Y_\delta Y_c$ in the region beyond open-loop crossover. The last two rows of Table 2 show the resulting approximations along with the "identified" dual-loop model parameters. Since the experimental data for the task with $K/s-2$ dynamics did not go beyond 10 rad/s, a time delay but no neuromuscular dynamics were included in the dual-loop model. Figures 13 and 14 show the favorable comparisons of measured and dual-loop model describing functions and, in the latter case, remnant spectrum. Note again the ability of the model to generate low-frequency phase

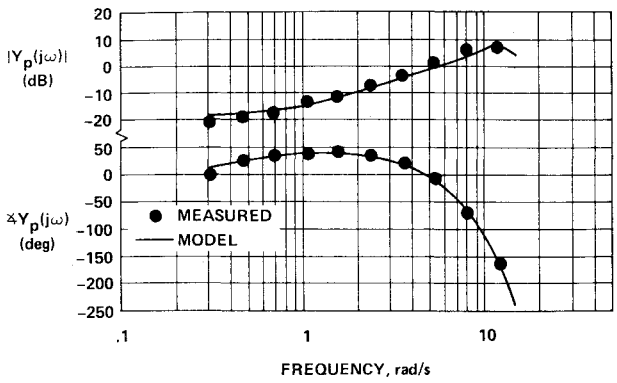

Fig. 13 Measured and dual-loop model describing functions for $K/(s^3 + 12.3s^2 + 11.6s)$ dynamics.

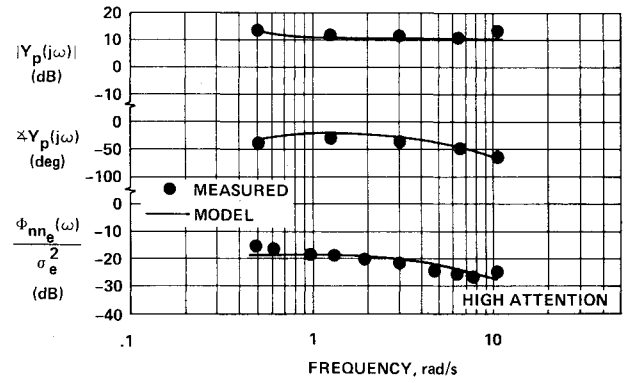

Fig. 14 Measured and dual-loop model describing functions and injected remnant spectra for $K/s - 2$ dynamics.

lag in the describing functions. No injected remnant measurements were reported in Ref. 10 for the third-order dynamics, so no remnant comparison was possible. Looking over the remnant models for the five tasks for which experimental remnant data were available, one sees that the low-attention model matches the data for the three *stable* controlled elements, whereas the high-attention model matches the data for the two *unstable* elements.

The ability of the dual-loop model to match experimental data when simplified internal representations of the controlled element are present is encouraging. Some insight into the reasons for the success of the simplified internal models is provided by considering the power spectral density of the control rate signal $\dot{u}_\delta$ for the two tasks just considered.

Figure 15 shows the exact controlled element transfer function for the third-order system along with the approximation valid beyond the open-loop crossover. Also shown is $\Phi_{\dot{u}\dot{u}_\delta}$, the power spectral density of $\dot{u}_\delta$ calculated from data of Ref. 10. By using the measured power spectrum for the control motion from Ref. 10, $\Phi_{\dot{u}\dot{u}_\delta}$ was calculated and plotted as shown. Note that the low-frequency inaccuracies of the approximate internal model will be mitigated by the fact that the power in the feedback signal $\dot{u}_\delta$ (the input to the $Y_\delta Y_c$ element) is concentrated in the frequency region beyond crossover where the approximate model is reasonably accurate. Similar results hold for the $K/s - 2$ dynamics and are discussed in Ref. 12.

Display-Manipulator Effects

In Ref. 12, the author discusses how the measured effects of some display and manipulator variations on human controller-describing functions, remnant and performance can be

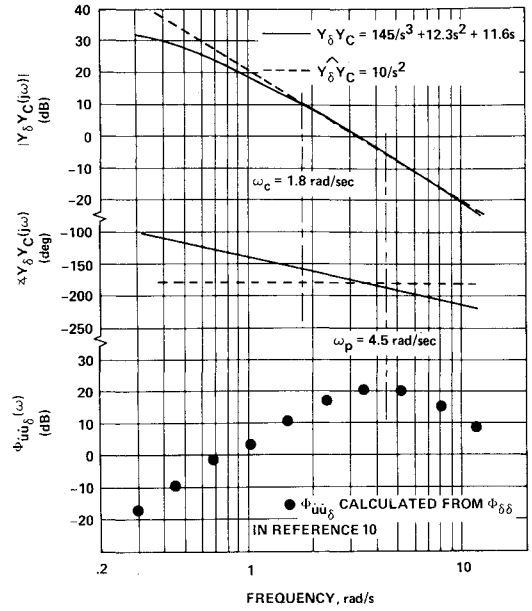

Fig. 15 Approximate and exact manipulator-controlled element dynamics and control-rate spectrum for $K/(s^3 + 12.3s^2 + 11.6s)$ dynamics.

explained via the dual-loop model. Specifically, the effects of peripheral viewing and displayed error quantization are shown to be consistent with the structure and hypotheses of the dual-loop model. Finally, the documented effects of depriving the human controller of force feedback by using an unrestrained manipulator are shown to be qualitively consistent with the assumption of kinesthetic feedback in the dual-loop model. A detailed discussion of these effects is beyond the scope of this paper. The reader is instead referred to Ref. 12.

Conclusions

There are four major attributes that a compensatory tracking model of the human controller should possess to be worthy of serious consideration. First, its frequency characteristics should resemble those of the well-known "crossover" model in the region of open-loop crossover.[1] Second, the model should exhibit τ_e variation, i.e., it should exhibit a larger effective time delay for tasks requiring (apparent) error lead equalization than for tasks requiring none. Third, the model should exhibit low-frequency phase lags. Finally, the model should exhibit isomorphisms with the human controller, i.e., the sensory inputs and structural elements of the model should be generally compatible with the physiological structure of the human.

As the author has attempted to point out in the preceding discussions, the dual-loop model possesses all of these attributes to one degree or another. What is particularly important, is that these attributes appear to be a natural consequence of the model structure itself, and the accompanying adaptive hypotheses.

The general paucity of high-frequency data in this study made the precise identification of the neuromuscular system parameters ζ_n and ω_n somewhat difficult. Consequently, no particular significance should be attached to the variations of these parameters in Table 2. The values should be considered approximate. This identification difficulty should not be interpreted as a weakness in the model formulation, however. Rather it indicates a certain robustness in the sense that variations in the open-loop neuromuscular system parameters do not have an appreciable effect upon the model characteristics with the inner loop closed. In terms of an acceptable control-system design, this is a highly desirable characteristic.

References

[1]McRuer, D. T., Graham, D., Krendel, E., and Riesener, W. Jr., "Human Pilot Dynamics in Compensatory Systems," Air Force Flight Dynamics Laboratory, AFFDL-TR-65-15, 1965.

[2]Gordon-Smith, M., "An Investigation into Certain Aspects of the Describing Functions of a Human Operator Controlling a System of One Degree of Freedom," *Proceedings of the Fifth Annual Conference on Manual Control*, March 1969, pp. 203-242.

[3]Stapleford, R. L., McRuer, D. T., and Magdaleno, R., "Pilot Describing Function Measurements in a Multiloop Task," NASA CR-542, 1966.

[4]Smith, R. H., "A Unified Theory for Pilot Opinion Rating," *Proceedings of the Twelfth Annual Conference on Manual Control*, May 1976, pp. 542-558.

[5]Smith, R. H., "A Theory for Handling Qualities With Applications to MIL-F-8785B," Air Force Flight Dynamics Laboratory, AFFDL-TR-75-119, 1976.

[6]Magdaleno, R. E., and McRuer, D. T., "Experimental Validation and Analytical Elaboration for Models of the Pilot's Neuromuscular Sub-system in Tracking Tasks," NASA CR-1757, 1971.

[7]Kleinman, D. L., Baron, S., and Levison, W. H., "An Optimal Control Model of Human Response, Part I," *Automatica*, Vol. 6, 1970, pp. 357-369.

[8]Wewerinke, P. H., "Human Operator Workload for Various Control Situations," *Proceedings of the Tenth Annual Conference on Manual Control*, April 1974, pp. 167-192.

[9]Levison, W. H., Elkind, J. I., and Ward, J. L., "Studies of Multivariable Manual Control Systems, A Model for Task Interference," NASA CR-1746, 1971.

[10]Levison, W. H., Baron, S., and Junker, A. M., "Modeling the Effects of Environmental Factors on Human Control and Information Processing," Aerospace Medical Research Laboratory, AMRL-TR-76-74, 1976.

[11]Jex, H. R. and Allen, R. W., "Research on a New Human Dynamic Response Test Battery," *Proceedings of the Sixth Annual Conference on Manual Control*, April 1970, pp. 743-777.

[12]Hess, R. A., "A Dual-Loop Model of the Human Controller in Single-Axis Tracking Tasks," NASA TM-73,249, May 1977.

From the AIAA Progress in Astronautics and Aeronautics Series..

AERODYNAMIC HEATING AND THERMAL PROTECTION SYSTEMS—v. 59

HEAT TRANSFER AND THERMAL CONTROL SYSTEMS—v. 60

Edited by Leroy S. Fletcher, University of Virginia

The science and technology of heat transfer constitute an established and well-formed discipline. Although one would expect relatively little change in the heat transfer field in view of its apparent maturity, it so happens that new developments are taking place rapidly in certain branches of heat transfer as a result of the demands of rocket and spacecraft design. The established "textbook" theories of radiation, convection, and conduction simply do not encompass the understanding required to deal with the advanced problems raised by rocket and spacecraft conditions. Moreover, research engineers concerned with such problems have discovered that it is necessary to clarify some fundamental processes in the physics of matter and radiation before acceptable technological solutions can be produced. As a result, these advanced topics in heat transfer have been given a new name in order to characterize both the fundamental science involved and the quantitative nature of the investigation. The name is Thermophysics. Any heat transfer engineer who wishes to be able to cope with advanced problems in heat transfer, in radiation, in convection, or in conduction, whether for spacecraft design or for any other technical purpose, must acquire some knowledge of this new field.

Volume 59 and Volume 60 of the Series offer a coordinated series of original papers representing some of the latest developments in the field. In Volume 59, the topics covered are 1) The Aerothermal Environment, particularly aerodynamic heating combined with radiation exchange and chemical reaction; 2) Plume Radiation, with special reference to the emissions characteristic of the jet components; and 3) Thermal Protection Systems, especially for intense heating conditions. Volume 60 is concerned with: 1) Heat Pipes, a widely used but rather intricate means for internal temperature control; 2) Heat Transfer, especially in complex situations; and 3) Thermal Control Systems, a description of sophisticated systems designed to control the flow of heat within a vehicle so as to maintain a specified temperature environment.

Volume 59—432 pp., 6 × 9, illus. $20.00 Mem. $35.00 List

Volume 60—398 pp., 6 × 9, illus. $20.00 Mem. $35.00 List

TO ORDER WRITE: Publications Dept., AIAA, 1290 Avenue of the Americas, New York, N.Y. 10019